www.lajss.org
Latin American Journal of Solids and Structures 4 (2007) 39–59

Parametrical analysis of extended endplate semi-rigid joints subjected to bending moment and axial force

P. C. da L. Nunes[1], L. R. O. de Lima[2,*], J. G. S. da Silva[3],
P. C. G. da S. Vellasco[2] and S. A. L. de Andrade[2]

[1] PGECIV, Post-Graduate Program in Civil Engineering, UERJ, Brazil
[2] Structural Engineering Department, State University of Rio de Janeiro, Brazil
[3]Mechanical Engineering Department, State University of Rio de Janeiro, Brazil

Abstract

Steel beam-to-column joints are often subjected to a combination of bending and axial forces. The level of axial forces in the joint may be significant such as in pitched-roof portal frames, sway frames or frames with incomplete floors. Current specifications that take in account the steel semi-rigid joint behaviour do not consider the simultaneous presence of axial forces (tension and/or compression) acting in the joints. On the other hand, an empirical limitation of 5% of the beam plastic resistance is the only limitation suggested in the Eurocode 3. In the cases where the axial force magnitude acting in the joint is less than this limit, its effects can be disregarded in the joint design. Despite this fact, the component method, proposed in the Eurocode 3, contemplate this situation since any component can be characterized, for any load type acting on the joint. This work presents a parametrical analysis of beam-to-column joints subjected to bending moment and axial force with the aid of a mechanical model based on the Eurocode 3 recommendations. The parametric analysis considers several factors that influence the joint global behaviour such as plate thickness, beam height, columns sections and the neutral axis position.

Keywords: semi-rigid joints, steel structures, extended endplate joints, bending moment, axial force and parametrical analysis.

1 Introduction

Structural steel joints are often designed as rigid or pinned. The first hypothesis implicates that there is no relative rotation between the connected members, i.e., the bending moment distribution occurs according to the connected members' flexural stiffness. Alternatively, when simple joint design is considered, the relative rotation of the connected members is liberated, i.e., the bending moment at the joints is zero. However, it is well-known that joints classified as rigid still present some flexural deformations while pinned joints can also possess some rotation restriction.

*Corresp. author email: lucianolima@uerj.br Received 28 August 2006; In revised form 30 October 2006

Usually, the beam-to-column joints are submitted to bending moment, shear and axial forces, while this last force is disregarded in most of the cases. However, in some structures, the presence of the axial forces in the joints affects directly its structural behaviour, such as:

- Regular frames under significant horizontal loading (seismic or extreme wind - Figure 1a), especially for sway frames;
- Irregular frames under gravity or horizontal loading, especially during the construction stage;
- Pitched-roof portal frames (Figure 1b).



(a)



(b)

Figure 1: Beam-to-column joint examples.

Some steel structures design codes already consider the semi-rigid joint behaviour, as the Eurocode 3, part 1.8 [11]. Despite this fact, this code only considers joints subjected to shear and/or bending moment, by imposing an empirical limitation of 5% of the beam plastic resistance as maximum axial force where the available recommendations are valid. However, it should be stressed that this empirical limit has no theoretical background to justify its use.

Aiming to determine the axial force influence over the beam-to-column semi-rigid joint response, some authors have proposed preliminary design models that were not properly validated or calibrated with experimental results. Among these works it is fair to mention the investigations made by Laurent [10], Jaspart [8, 9], Silva & Coelho [6] and Cerfontaine [1, 2].

Only Wald [12], Silva *et al.* [5] and Lima *et al.* [7] performed experimental tests on beam splices, extended and flush endplate beam-to-column joints subjected to bending moment and tension/compression axial force, respectively.

This work presents a comparison between the experiments made by Lima et al. [7]and the results obtained with the application of the mechanical model proposed by Cerfontaine [1, 2] for

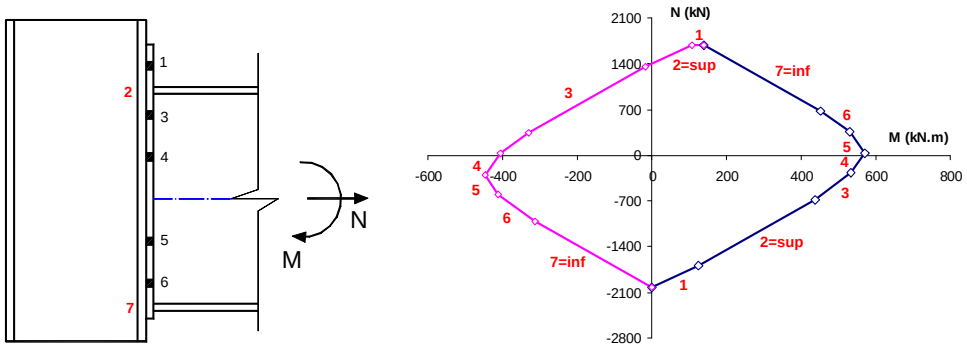
endplate beam-to-column joints subjected to bending moment and tension/compression axial force [3]. The following section presents a brief description of the analytical model that was used in throughout the present work.

2 Analytical model description

Cerfontaine [1,2] developed an analytical model based on the Eurocode 3 [11] component method for the characterization of beam-to-column joints or beams splices subjected to bending moment and axial forces. This model will be briefly described in the current section while additional information can be obtained in Cerfontaine [1, 2], Nunes [3] and Nunes et al. [4].

2.1 Interaction diagram characterization

The first step of the design model consists in determining a bending moment versus axial force interaction diagram for the investigated extended endplate bolted joint. This diagram defines a curve where the couple bending moment / axial force applied to the joint is situated representing a limit to the structural collapse. Obviously if this couple is located outside of the area delimited by this curve, the joint collapse is reached. Figure 2 presents an example of an interaction diagram for an extended endplate joint with five bolt rows where positive bending moment and the axial force acting in the joint are highlighted.



(a) extended endplate joint (b) interaction diagram

Figure 2: Extended endplate joint interaction diagram.

This interaction curve can be analytically defined for any bolted joint, being characterized by N bolt rows under tension and two lines in compression (in beam top and bottom flanges directions) resulting in n = N + 2 lines in total. It is also important to emphasize that the bolt rows can only be used when subjected to tension axial forces.

The current model assumes that all of the lines and, consequently, all the components possess an unlimited ductility capacity. As only the joint response at collapse and the ductile behaviour

hypothesis is here considered, a perfectly plastic analysis strategy was used This analysis is based on the determination of an internal force distribution that is in equilibrium with the external forces, still satisfying the collapse criteria. Consequently, the determination of the joint resistance implies that the collapse force distribution satisfies the equilibrium equations. The bending moment M and axial force N, acting on the joints ca be obtained with the aid of eq. (1).

$$M = \sum_{i=1}^{n} h_i \cdot F_i \text{ and } N = \sum_{i=1}^{n} F_i \tag{1}$$

where F_i and h_i represent the i-line resistance and the lever arm respectively. The acting joint forces M and N are located at the beam mid-height.

The bending moment and the axial force are related by the definition of an eccentricity e equals to the bending moment to axial force ratio, i.e., e= M/N. At this stage, it is necessary to establish the resistance criteria for the various joint different lines, according to the Eurocode 3 recommendations [11]. In order to define the bolt row stiffness, for instance, it is necessary to determine the stiffness coefficient and the elastic limit of the different components considered at each line. Therefore, each row will be modelled by a series of springs that represent each of these components, where the row resistance is equal to the resistance of weakest component present in this row. It is also important to emphasize that group effects should also be considered between two bolt rows [m,p] establishing the value for the group resistance F_{mp}^{Rd}. Therefore, it is convenient to describe the components' resistance criteria that the acting joint forces should satisfy:

$$\sum_{i=m}^{p} F_i \leq F_{mp}^{Rd\alpha} \quad m = 1, \ldots, p \text{ and } p = m, m+1, \ldots, n \tag{2}$$

where $F_{mp}^{Rd\alpha}$ is the group resistance including the m to p rows for the α component. In cases where m is equal to p, $F_{mp}^{Rd\alpha}$ is the m-line individual resistance for the α component.

Starting from the equilibrium equations and the lines collapse criteria, a step by step application of the static theorem generates:

> "The interaction criterion between the bending moment (M) and the axial force (N) at collapse is described by a group of 2n straight line parallel segments, two by two, whose inclination angle is respectively the n-rows lever arm (h_k). Along these segments, the force (F_k) varies between zero and the maximum row resistance, defining two segment points" [1, 2].

It can be noticed that the resistances of the rows (F_i^{Rd+} and F_i^{Rd-}) are differently defined according to the i index that can be less (F_i^{Rd+}) or greater (F_i^{Rd-}) than k. Interaction diagram notable points can be determined with the aid of the above mentioned procedures. The bending moment axis of the interaction diagram corresponds to an eccentricity equal to zero while the

axial force axis represents an infinite (positive or negative) eccentricity. A detailed description of the procedures used for the determination of the various interaction diagram notable points for an extended endplate joint will be presented in the following sections.

2.2 Bending moment versus rotation curve characterization

The interaction diagram determination, as previously mentioned, is based on the components ductility hypothesis. The components' ultimate resistance is not dependent on the combination of the bending moment and axial force that is acting on the joint. However, the joint initial stiffness, or the joint elastic behaviour induced by this load combination, is not yet known. To obtain these characteristics, it is necessary to determine each component elastic behaviour present in every bolt row to be considered. The characterization of a α component elastic behaviour is obtained with the equations presented below and it can be seen in the Figure 3.

$$\begin{gathered} F_i < F_i^{el\alpha} \rightarrow F_i = K_{i,ini}^{\alpha}.\Delta_i^{\alpha} \\ F_i^{el\alpha} < F_i < F_i^{Rd\alpha} \rightarrow F_i = K_i^{\alpha}.\Delta_i^{\alpha} = \left[K_{ii,ini}^{\alpha} \cdot \left(\frac{F_i^{el\alpha}}{F_i} \right)^{2.7} \right] \cdot \Delta_i^{\alpha} \end{gathered} \tag{3}$$

where $F_i^{el\alpha}$, $K_{i,ini}^{\alpha}$ and Δ_i^{α} represents, for the α component of the i-row, its elastic limit, initial stiffness and displacement, respectively.

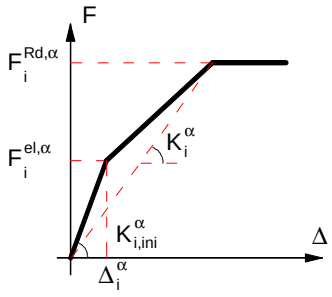


Figure 3: Constitutive law for a general component.

The column flange in bending and endplate in bending components resistance are characterized by a bolted T-Stub behaviour with three different collapse mechanisms, as described in Eurocode 3 [11], i.e., full flange yielding without bolt failure (mode 1), flange yielding with bolt failure (mode 2) or simply bolt failure without flange yielding (mode 3). When the component resistance is associated to the first or second modes this value is greater than 95% of the tension bolt row resistance, leading the components not to possess enough ductility and the elastic limit to be defined as 2/3 of this resistance. When the failure is associated to the third mode, i.e., bolt failure, the elastic limit is made equal to the brittle component resistance $\left(F_i^{Rd,\alpha}\right)$. For

the other cases, the components present enough ductility and an elastic limit equals to 2/3 of the component resistance is assumed.

As presented in Eurocode 3 [11], as soon as all the components behaviour present in a bolt row are known, these values can be associated as springs connected in series. This is followed by an evaluation of the displacement maximum values at the elasto-plastic limit and, later, at the collapse. With these values in hand, the joint initial stiffness can be evaluated, as well its bending moment capacity.

However, the neutral axis position is not yet known. This point location is fundamental for determining which lines contribute to the joint initial stiffness. Considering the initial joint configuration, a linear relationship exists between the displacements of the i-row and a reference displacement, Δ. This displacement is conventionally chosen in relation to the neutral axis position (h=0). The i-row displacement can be later determined in terms of the joint section rotation (φ):

$$\Delta_i = \Delta + h_i \cdot \varphi \tag{4}$$

where Δ_i is the i line displacement, Δ is the joint displacement, h_i is the i line lever arm and φ the global joint rotation, respectively.

The displacement (Δ) defines, in a unique way, the joint displacement state, where it is also interesting to define the neutral axis position point (Δ_0) and its corresponding lever arm (h_0). As it is well-known, this point also defines the change in sign of the line displacements:

$$\begin{gathered} \Delta_0 = 0 = \Delta + h_0 \cdot \phi \Rightarrow h_0 = -\frac{\Delta}{\varphi} \\ \Delta_i = (h_i - h_0) \cdot \varphi \quad \forall i \end{gathered} \tag{5}$$

The initial stiffness evaluation involves:

- the equations that characterize the each line elastic behaviour evaluated according to Eurocode 3 recommendations [11];
- the linear relationship that describes the each line displacements given by eq. (4);
- the equilibrium equations given by eq. (1);
- the eccentricity definition "e" and the joint neutral axis position, eq. (5), in the elastic domain, h_0^{el}.

These steps define the equation that evaluates the joint initial stiffness (K_M^{el}):

$$K_M^{el} = \left(\frac{M}{\phi}^{el}\right) = \sum K_{i,ini}.h_i \left(h_i - h_0^{el}\right) = e.\sum K_{i,ini}.\left(h_i - h_0^{el}\right) \tag{6}$$

Starting from the eq. (6), the equation for the eccentricity in function of the lever arm h_0^{el} can be obtained:

$$e = \frac{\sum K_{i,ini}.h_i\left(h_i - h_0^{el}\right)}{\sum K_{i,ini}.\left(h_i - h_0^{el}\right)} \quad \text{or} \quad h_0^{el} = \frac{\sum K_{i,ini}.h_i\left(h_i - e\right)}{\sum K_{i,ini}.\left(h_i - e\right)} \tag{7}$$

When a row reaches its elastic limit, the row elastic force distribution corresponds to an elastic axial force N^{el} and an elastic bending moment, as well as a displacement Δ^{el} and an elastic rotation φ^{el}. Having these values in hand, the elastic bending moment, the displacement and the rotation are defined by:

$$M_{el} = K_M^{el}.\min\left(\frac{F_j^{el}}{\left(h_j - h_0^{el}\right).K_{j,ini}}\right) \ \forall j, F_j \neq 0; \ \ \Delta^{el} = \frac{N^{el}}{K_N^{el}} \ \text{ and } \ \varphi^{el} = \frac{M^{el}}{K_M^{el}} = \frac{-\Delta^{el}}{h_0^{el}} \tag{8}$$

A structural joint is characterized by three collapse forms where the first is related to an excessive tension force in one of its bolt rows. The second mode is associated to an excessive compression force that can affect the compression components without unloading the bolt applied force. Finally, the third mode is related to an unload phase in the bolt rows after reaching the compression row resistance. The study of these different collapse modes makes possible to express the joint displacements state at collapse. As in the joint elastic behaviour phase, it is interesting to obtain the position of the neutral axis point in the ductile collapse state as well as the associated joint secant stiffness:

$$h_0^{Rd} = -\frac{\Delta^{Rd}}{\varphi^{Rd}} \ \text{ and } \ K_M^{Rd} = -\frac{M^{Rd}}{\varphi^{Rd}} \tag{9}$$

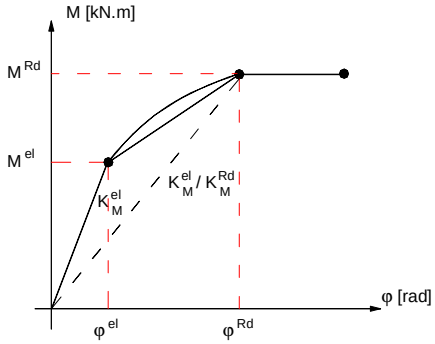


Figure 4: Joint behaviour curves (M x φ).

Finally, complete bending moment versus joint rotation curve can be obtained, Figure 4. It is important to observe that the column web in shear component (1) have to be individually considered [3] as it can be seen in the mechanical model illustrated in Figure 5.

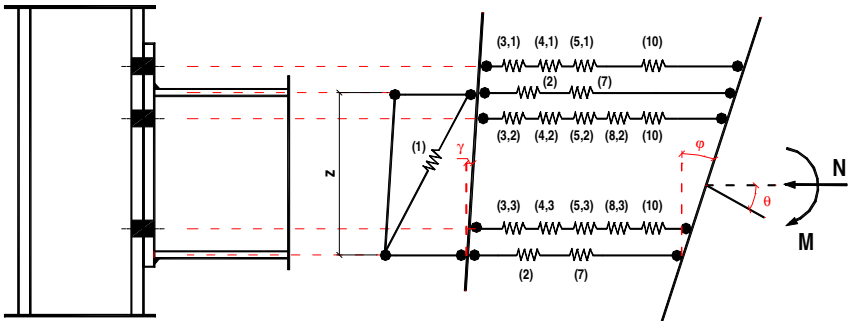


Figure 5: Mechanical model [1, 2].

3 Analytical model and experimental results comparison

The application of the model, previously described, was made in an extended beam-to-column joint, Figure 6, that was tested by Lima et al. [7] at the Structural Mechanical Laboratory of the University of Coimbra, Portugal. This figure presents the joint geometrical properties as well as the load application system that defines the applied bending moment and compression axial force. Seven experimental tests will be used for comparison with the analytical results where the level of active axial force was varied in the joint (positive or negative) as described in the Table 1. Another important issue investigated was the individual influence of the column web in shear component. This hypothesis was considered in all the bending moment versus rotation curves that will be later presented.

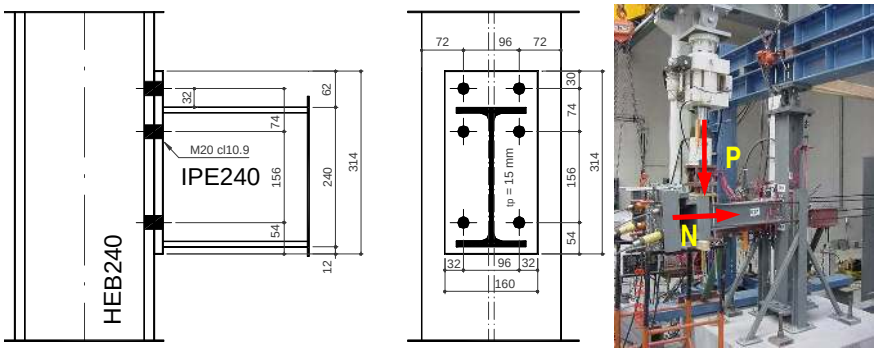
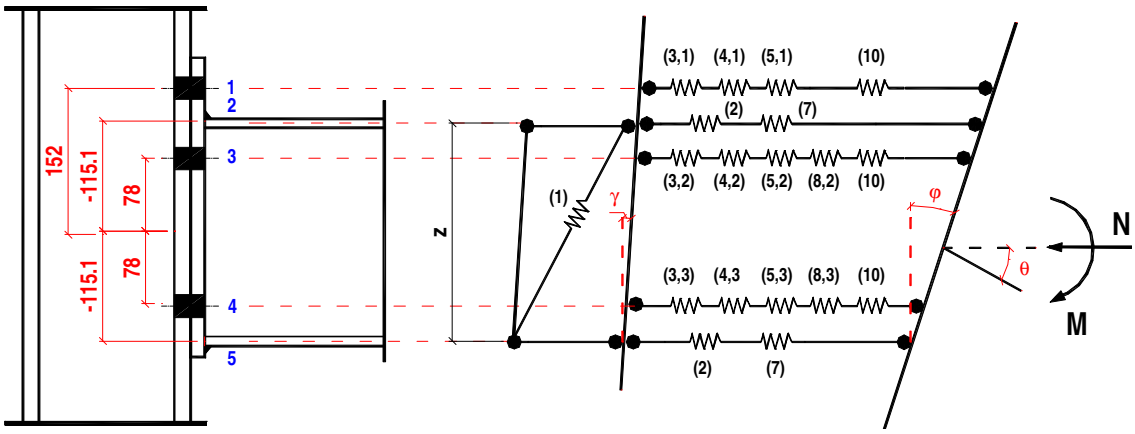


Figure 6: Extended endplate beam-to-column joint (Lima *et al.*, 2004).

The model used to characterize the joint according to the Eurocode 3 [11] and the rows considered in the model proposed by Cerfontaine [1, 2] can be observed in the Figure 7. In this model, the relevant components are: (1) column web panel in shear, (2) column web in compression, (3) column web in tension, (4) column flange in bending, (5) endplate in bending,

Table 1: Joints experimental results.

Joint Response	EE2	EE3	EE4	EE5	EE6	EE7
M (kN.m)	125.4	113.2	111.9	118.1	97.1	86.1
N (kN)	-137	-260	-363	-195.4	130.6	257.1
e (mm)	-915.33	-435.39	-308.26	-604.40	743.49	334.89
% N_{pl}	-10	-20	-27	-15	+10	+20



(a) Lever arms [2] (b) mechanical model [11]

Figure 7: Mechanical model characterization.

(7) beam flange and web in compression, (8) beam web in tension and (10) bolts in tension. It is important to observe that the model proposed by Cerfontaine [1, 2], considers that the rows situated below the beam mid-height are associated to negative lever arms. This is not made in the Eurocode 3 [11] where all bolt lines are associated to positive lever arms.

The use of the analytical model starts with an initial joint design according to the component method proposed in the Eurocode 3 [11] using the mechanical properties presented in the Table 2. This preliminary design considered the mechanical model depicted in Figure 7 and it resulted in the values presented in the Table 3. It is important to observe out that these results have not incorporated the column web in shear component (1). This strategy was used because its behaviour is independently from the other joint components. After the identification of the weakest component for every bolt row that was considered, the final resistance of each bolt lines can be determined (Table 4).

The interaction diagram for this joint, illustrated in Figure 8, do not depend on the acting joint loads. The numbers presented beside each straight line segment indicate, for a certain level of M and N, which bolt row controls the collapse.

Table 2: Steel mechanical properties

Specimen	f_y (MPa)	f_u (MPa)	E (MPa)
Nominal Value	275	430	210000
Beam web	363.43	454.25	203714
Beam flange	340.14	448.24	215222
Column web	372.02	477.30	206936
Column flange	342.95	448.79	220792
Endplate	369.44	503.45	200248
BOLTS – M20			
Nominal value	900	1000	210000
Mean value	939.67	1018.67	-

Table 3: Components resistances for each bolt row (individual and as part of a group).

Component	individual					group		
	1,1	2,2	3,3	4,4	5,5	3,4	1,3	1,4
(8) BWT	-	-	493	493	-	**765**	-	-
(5) EPB	**290**	-	**341**	**341**	-	341	-	-
(4) CFB	408	-	408	408	-	784	**714**	**749**
(3) CWT	533	-	533	533	-	834	735	-
(7) BFC	-	**542**	-	-	**542**	-	-	-
(2) CWC	-	680	-	-	680	-	-	-
(10) BT	441	-	441	441	-	-	-	-

Table 4: Bolt row resistances (in kN).

i	h_i (mm)	$F^{Rd}_{(i,i)}$	$F^{Rd}_{(i-1,i)}$	$F^{Rd}_{(i-2,i)}$	$F^{Rd}_{(i-3,i)}$
1	152.0	290	-	-	-
2	115.10	542	-	-	-
3	78.0	341	-	714	-
4	-78.0	341	765	-	749
5	-115.1	542	-	-	-

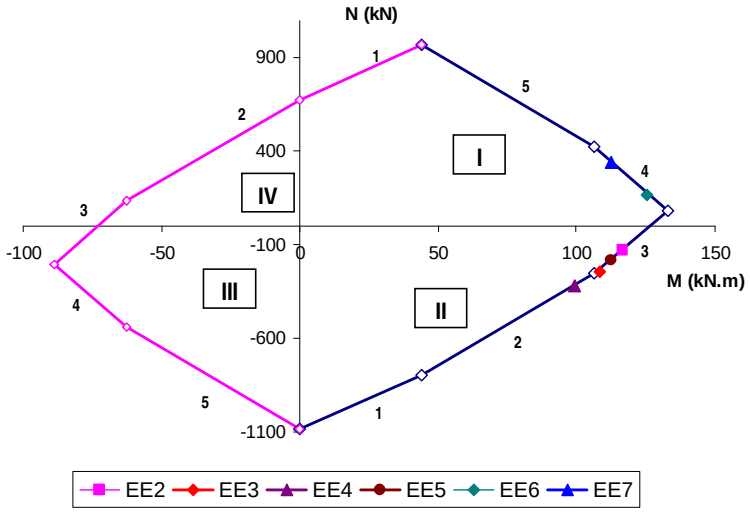
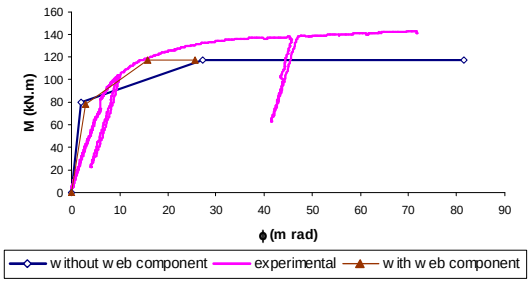


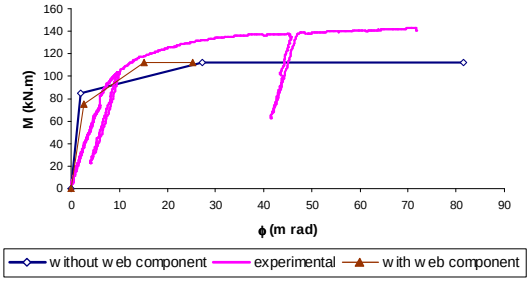
Figure 8: Moment versus axial force iteration diagram

The iteration diagram determination starts on point (0;-1084kN) that is associated with the maximum negative axial force joint response (N^{-}_{max}) and its associated bending moment equals to zero. This value of N^{-}_{max} corresponds to twice the compression row weakest resistance, i.e., beam flange in compression (7) as observed in Table 3. The first straight line segment is obtained with the point characterized by the influence of the mechanical model first line, i.e. the external bolt row. The axial force at this point is determined by removing the first line weakest resistance contribution (-1084 kN + 290 kN = -794 kN) and its corresponding bending moment, 290 kN multiplied by the first bolt row lever arm, i.e., 152 mm, resulting in 44.08 kN.m. The other diagram points are obtained, up to the fifth and last segment, by the successive consideration of the other bolt rows resistances. The other half of the diagram determination begins with the model bottom row that characterizes a bending moment that induces tension in the beam bottom flange. The second point of the first straight line segment was obtained considering the contribution of the bottom flange. The axial force is calculated subtracting the weakest compression resistance from the beam plastic axial resistance (-1084kN + 542kN = -542kN). The associated bending moment resistance was obtained multiplying this compression resistance by the respective lever arm(-542kN x 0.115m=62.3kN.m).

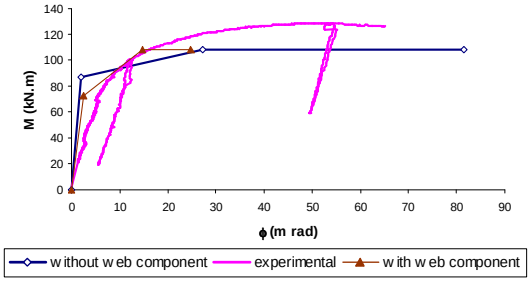
Starting from this interaction diagram, the next step consists in identifying the intersection between the straight line that characterizes the experimental test eccentricity and its corresponding line in the diagram, Figure 8. With the aid of the interaction diagram it is also possible to identify the straight line that corresponds to the evaluated eccentricity (e=M/N) and, using the model presented previously, its associate moment versus rotation curve can be determined. This was the procedure used to evaluate the seven experimental bending moment *versus* rotation curves illustrated in Figure 9.



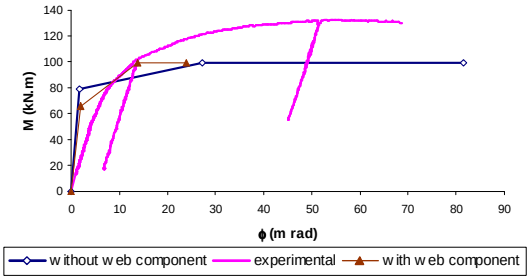
(a) EE2 (N = - 137.0 kN = 10% N_{plbeam})



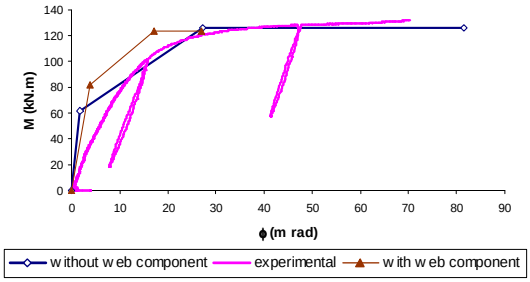
(b) EE5 (N = -195.4 kN = 15 % N_{plbeam})



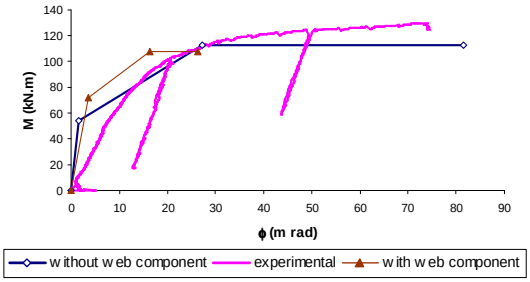
(c) EE3 (N = -260.0 kN = 20 % N_{plbeam})



(d) EE4 (N = -363.0 kN = 27 % N_{plbeam})



(e) EE6 (N = +130.6 kN = 10 % N_{plbeam})



(f) EE7 (N = +257.1 kN = 20 % N_{plbeam})

Figure 9: Analytical and experimental comparisons in terms of moment versus rotation curves.

The blue curve present in tests EE2 to EE5, where the bending moment is positive and the axial force is negative, was obtained through the analytical model disregarding the column web in shear component contribution. As soon as this component increases it can be noticed that the analytical curves fit better with the tests results. The results comparison indicated that the experiments values were greater than its analytical counterparts, being an inferior limit for the studied problem.

The column web component directly influences the joint global behaviour, specially in terms of the joint ultimate flexural capacity. This occurs because this component is directly affected by the applied axial force load level since this level modifies the z lever arm considered in design. Tests EE6 and EE7, where the bending moment and the axial force are positive, produced

analytical model curves with a greater stiffness than its corresponding tests values. However, it is important to observe that the analytical model was accurate to predict the tested joint flexural capacities.

When a positive axial force is considered in the analytical model, the generated curve produce joint initial stiffness values greater than the experiments indicating that further calibrations are still necessary for this case. Generally, the analytical model produced satisfactory results when compared to the experiments. This was the main motivation for a parametrical analysis that will be presented in the next section.

4 Parametrical analysis

This item presents a parametrical analysis performed on extended endplate joints subjected to bending moment and axial forces (tension/compression) using the analytical model proposed by Cerfontaine [1, 2]. The results are presented in terms of the relevant changes observed in the joint global behaviour expressed by their respective interaction diagram. This diagram defines the boundaries within the couple of acting bending moment (M) and axial force (N) have to be limited to avoid the joint structural failure. It is important to observe that the joints were designed according to component method proposed in the Eurocode 3 [11] previously described. The following alternatives were considered in the parametric analysis:

1. Varying the beam height for a fixed column cross section (HEB240) and endplate thickness;
2. Varying the column cross section for a fixed beam section (IPE240) and endplate thickness;
3. Varying the endplate thickness while maintaining the beam cross section (IPE240), the column cross section (HEB240) and the endplate dimensions;
4. Varying the eccentricity values (M/N) to generate different joint neutral axis locations.

The geometrical characteristics used in the parametrical analysis are depicted in Figure 10 while Table 5, presents the adopted joint dimensions and spacing. The same material mechanical properties described in the earlier sections were used in this study.

4.1 Beam height

The first parametrical analysis is related to the influence of the beam height over the M versus N interaction diagram. As previously mentioned, the adopted geometrical properties are present in the Table 5. When the IPE240 steel profile was used, the endplate width (b) was made equal to 150mm instead of 140mm due to endplate hole/edge spacing limitations. Its respective interaction diagram is presented in the Figure 11, where the diagram asymmetry can be explained by the adopted joint geometry. It can be observed that the varying the beam height implies in

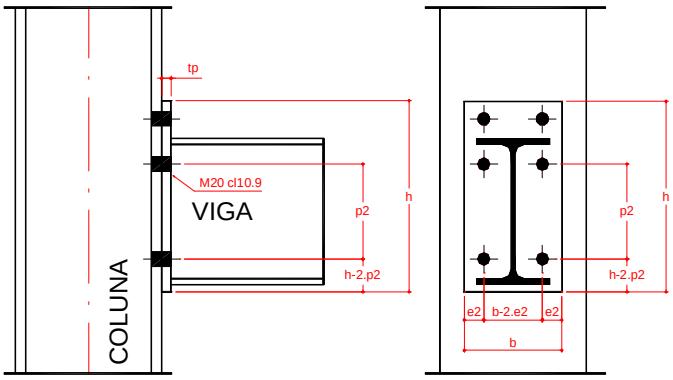


Figure 10: Endplate beam-to-column joint variables.

Table 5: Joint geometrical characteristics (in mm).

Beam section	h_{beam}	$h_{endplate}$	b	p_2	e_2
IPE 240	240	340	150	127	27
IPE 300	300	400	180	187	42
IPE 400	400	500	200	287	52
IPE 500	500	600	220	387	62
IPE 600	600	700	240	487	72

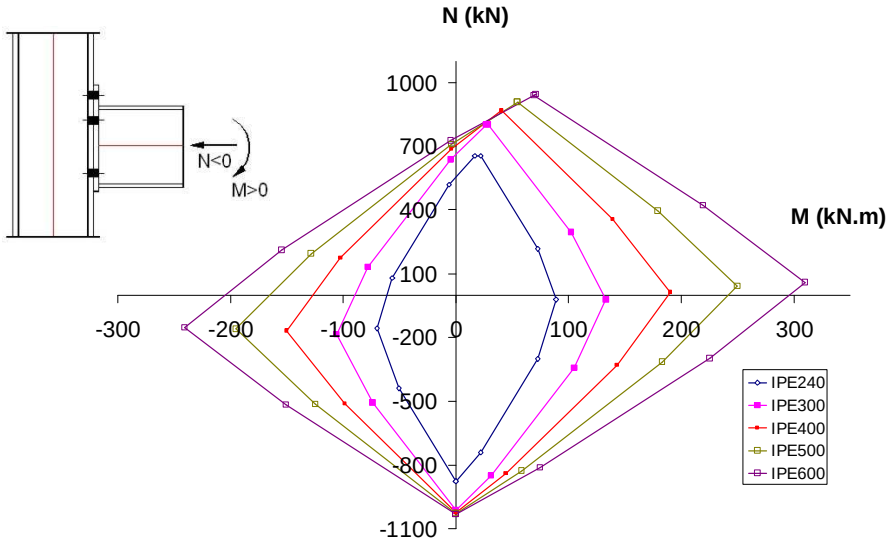


Figure 11: Moment versus axial force iteration diagram for various beam heights.

Table 6: Individual components resistances (in kN) (beam height variation).

Beam Section	Tension										
	3,1	4,1	5,1	3,3	4,3	5,3	8,3	3,4	4,4	5,4	8,4
IPE240	394.2	369.3	136.7	394.2	369.3	297	317.2	394.2	369.3	297	317.2
IPE300	394.2	376.3	182.3	394.2	376.3	342.4	514.9	394.2	376.3	342.4	514.9
IPE400	394.2	376.3	182	394.2	376.3	342	515	394.2	376.3	342	515
IPE500	394.2	376.3	200.5	394.2	376.3	353.9	596.6	394.2	376.3	353.9	596.6
IPE600	394.2	376.3	218.7	394.2	376.3	362.9	640.6	394.2	376.3	362.9	640.6

Beam Section	Compression		
	1	2	7
IPE240	475	506.3	438.4
IPE300	475	507.4	597
IPE400	475	511	929.9
IPE500	475	514.1	1247
IPE600	475	515.6	1315

the generation of different and very well defined curves. The following paragraphs will present a detailed analysis of this diagram in terms of the variation of each individual component resistance determined with the aid of the component method proposed in the Eurocode 3 [11].

The Table 6 illustrates the component resistance for the joint used in this parameterization. A closer inspection of the components resistance indicates that varying the beam height do not affect the resistances of the column web in tension (3,1, 3,3 and 3,4) and column web in shear (1) components.

It is important to reiterate that the first component column web in shear (1) does not influence the interaction diagram. This is explained because this component is only considered for obtaining of the bending moment versus rotation curve of a interaction diagram singular point. Despite this fact, their values were still presented to exemplify the variation of all the components involved in the joint model.

The column flange in bending component (4,1, 4,2 and 4,3), tended to reach a constant value for beam profile greater or equal to the IPE300 profile because from this point onwards, the component effective width is controlled by the flange column width that was not altered at this stage of the parametrical analysis.

A closer inspection of the interaction diagrams indicates that the point corresponding to the maximum negative axial force (0;-876.85kN), have not varied significantly from the beam IPE300 (0;-1014.8kN), even when a IPE600 section was used. In fact, checking the joint compression region components values, i.e., components (1), (2) and (7), it is easy to identify that the second component (2), column web in compression, controls the joint design. This shows that the axial force resistance of the joints is limited by this component, even for beams whose resistance to

these forces are greater (according to the observation of the column response regarding the beam flange in compression component).

A variation of other components resistances was noticed like the endplate in bending (5,1, 5,3 and 5,4) or the beam web in tension (8,3 and 8,4), but, despite this fact, no significant change was noticed in the interaction diagrams. On the other hand, a proportional increase of the joint flexural resistance in terms of an increase of the beam cross section increase was noticed. This is easily explained because the active forces lever arm in the tension bolt rows is also increased.

The beam web in tension component (8,3 and 8,4), has its resistance determined by the column web in tension component (3). This component is evaluated considering the joint tension region where the beam flange tension force is applied. Despite having a significant resistance increase with an increase of the beam section, there is no direct influence over the interaction diagram because other components still control the design at the joint tension region.

4.2 Column cross section

Figure 12 depicts M x N interaction diagrams related to the column cross section variation while Table 7 presents the individual components resistances for the adopted columns cross sections.

Table 7: Individual components resistances (in kN) (column cross section).

Column Section	Tension										
	3,1	4,1	5,1	3,3	4,3	5,3	8,3	3,4	4,4	5,4	8,4
HEB200	317.8	340.7	136.7	317.8	340.7	297	332.9	317.8	340.7	297	332.9
HEB240	333.2	395.8	136.7	333.2	395.8	297	332.9	333.2	395.8	297	332.9
HEB300	292.1	441.0	136.7	292.1	441.0	297	332.9	292.1	441.0	297	332.9
HEB400	1104	441.0	136.7	1104	441.0	297	332.9	1104	441.0	297	332.9
HEB500	1598	441.0	136.7	1598	441.0	297	332.9	1598	441.0	297	332.9

Column Section	Compression		
	1	2	7
HEB200	355.1	395.2	438.4
HEB240	475	506.3	438.4
HEB300	676.6	676.3	438.4
HEB400	1003	935.7	438.4
HEB500	1289	1107	438.4

The initial point of the diagram corresponds to the beam axial resistance. An inspection of Figure 12, indicates that for the first case (HEB200), the column web in compression component (2) controls the joint compression region design since the column web in shear component (1) was not considered. Therefore, this diagram point is defined by the couple (0;2 x 395.2kN = -790.4kN). From the second profile (HEB240) onwards, the beam flange in compression com-

ponent (7) starts to control the compression region joint design leading all interaction diagram points to converge for a single value equal to 876.84kN (2 x 438.42kN).

The endplate in bending (5) and beam web in tension (8) components of the joint tension region, have not changed since the beam cross section and the endplate thickness were not altered. As the endplate in bending (5) is the controlling design component of this joint region, all initial straight lines of the interaction diagram coincides from the column HEB240 onwards.

When the data related to the column flange in bending component (4) in the Table 7 is observed, it is possible to verify that a constant value of 441kN was achieved for column cross section larger or equal to HEB300. This happens because this component is characterized by a bolted T-Stub behaviour. This implies that a column flange thickness increase can increase this component resistance until the failure limit of the third mode mechanism is reached, i.e., bolts in tension failure. From this point, altering the column profile does not affect the component resistance.

The beam web in tension component resistance (3), as expected, is proportional to an increase of the adopted column cross section. However, as this component does not control the tension region joint design, it also does not alter the interaction diagram shape.

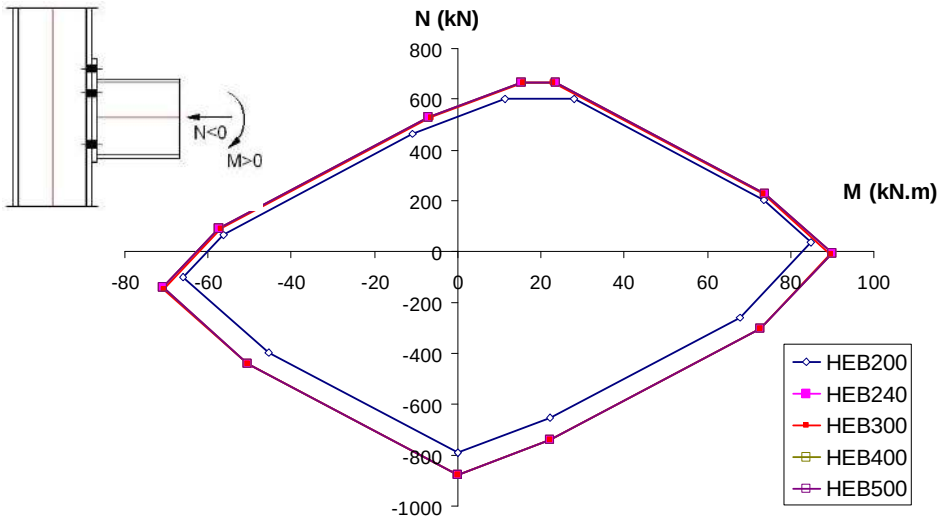


Figure 12: Moment versus axial force iteration diagram for various column cross sections.

4.3 Endplate thickness

The parametrical analysis also considered endplate thicknesses varying from 10 up to 25 mm. Their respective interaction diagram are presented in the Figure 13 while the components individual resistances are depicted in Table 8.

An observation of Table 8, indicates that only the endplate in bending (5) and column web

in compression (2) components had their resistance values modified. This occurs due to the fact that the endplate in bending component is characterized by the formation of collapse mechanisms based on the bolted T-Stub response. This means that an endplate thickness increase implies in a resistance increase until an endplate thickness equals to 20mm is reached.

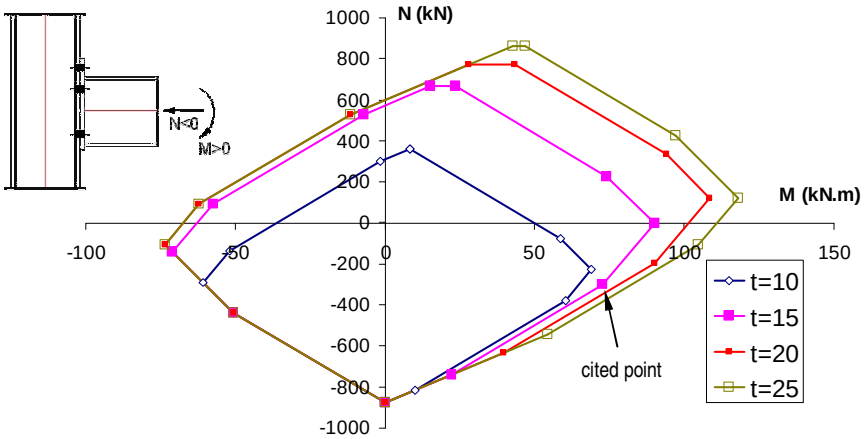


Figure 13: Moment versus axial force iteration diagram for various endplate thicknesses.

Table 8: Individual components resistances (in kN) (endplate thickness)

Endplate thickness	Tension										
	3,1	4,1	5,1	3,3	4,3	5,3	8,3	3,4	4,4	5,4	8,4
10mm	333.2	395.8	60.8	333.2	395.8	149.8	333.2	333.2	395.8	149.8	332.9
15mm	333.2	395.8	136.7	333.2	395.8	297	333.2	333.2	395.8	297	332.9
20mm	333.2	395.8	243	333.2	395.8	366.3	333.2	333.2	395.8	366.3	332.9
25mm	333.2	395.8	333	333.2	395.8	441	333.2	333.2	395.8	441	332.9

Endplate thickness	Compression		
	1	2	7
10mm	475	505.2	438.4
15mm	475	514.1	438.4
20mm	475	522.7	438.4
25mm	475	531.1	438.4

However, when a thickness of 25mm is adopted, the third mode controls the component collapse while its capacity is made equal to the bolt in tension component resistance. As this component controls the joint tension region design, an inspection of the interaction diagram (Figure 13), it can be seen that after the marked point , great differences in behaviour occur. Such differences are proportional to the resistance of the first row endplate in bending component

(5,1).

The column web in compression component (2) changes are justified due to the fact that the column web is subject to concentrated forces transmitted by the beam top and bottom flanges induced by the bending moment. This fact induces tension at the joint upper region, whose of the effective width calculation considers the force dispersion angle. This way, as great is the endplate thickness, great will be the effective width of the column web submitted to the compression. However, this difference does not induce changes in the interaction diagram because the joint compression region is controlled by the beam flange in compression component (7).

4.4 Neutral axis position

It is also interesting to evaluate the changes to the joint neutral axis location in terms of the applied load eccentricities (e=M/N), Figure 14.

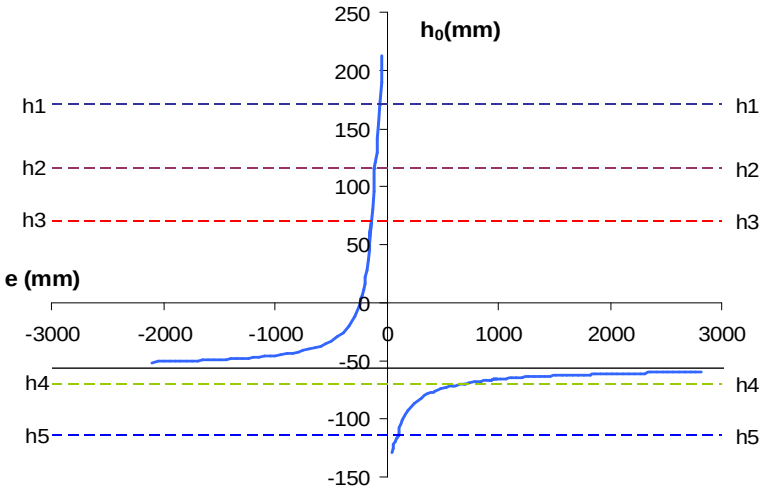


Figure 14: Moment/axial force ratio *versus* neutral axis position.

In this graph a horizontal asymptote close of the mechanical model fourth line (h ≈ 60mm) is clearly identified. The neutral axis position is always located below the horizontal asymptote for axial force values that induces compression at the joint and bending moment that generates tension in the beam top flange, i.e. positive eccentricity "e" values. The reverse situation occurs for negative eccentricities (when the axial force and the bending moment have different signs) with the neutral axis location situated above the already mentioned asymptote axis.

5 Concluding remarks

This work presented a parametrical analysis of extended endplate beam-to-column joints subjected to bending moment and axial forces using the analytical model proposed by Cerfontaine [1, 2]. The model validation was made by comparisons to bending moment *versus* rotation curves of seven experimental tests. These tests were made by Lima *et al.* [7] on beam-to-column extended endplate joints varying the joint axial force and bending load levels.

The analytical model results were in agreement with the experiments. Small differences found in the initial stiffness of the bending moment versus rotation curves were observed. Considering the column web component, a better fit of the analytical with the test curves was observed.

The parametrical analysis showed that the varying the beam cross sections did not affect the resistances values of the column web in tension (3) and column web in shear (1) components. The beam section change have also not produced significant modifications on the interaction diagram inferior point, even when a IPE600 cross section was used. This happened because the compression component that controlled the joint design was the column web in compression (2) as can be observed in Table 5.

The increase in the joint flexural capacity was proportional to the increase of the beam section due to the correspondent increase of the active forces lever arm in the tension bolt rows. The columns section change indicated that, in the first case (HEB200), the controlling joint design component was the column web in compression (2). From the second case (HEB240), the beam flange in compression component (7) controlled the joint compressive region design. This was the main reason for all interaction diagram lower points converged for the same value.

Acknowledgements: The authors would like to thank FAPERJ, CAPES and CNPq, for the financial support provided for the present investigation.

References

[1] F. Cerfontaine. Etude analytique de l'interaction entre moment de flexion et effort normal dans les assemblages boulonnés. *Construction Méttalique*, (4):1–25, 2001.

[2] F. Cerfontaine. Etude de l'interaction entre moment de flexion et effort normal dans les assemblages boulonn. Master's thesis, Faculté des Sciences Appliquées - University of Liège, Belgium, 2004. Thèse de Docteur en Sciences Appliquées.

[3] P. C. da L. Nunes. Análise paramétrica de ligações com placa de extremidade em estruturas de aço submetidas a momento fletor e força axial. Master's thesis, Faculdade de Engenharia - FEN/UERJ, 2006.

[4] P. C. da L. Nunes, L. R. O. de Lima, P. C. G. da S. Vellasco, S. A. L. de Andrade, and J. G. S. da Silva. Modelagem de ligações semi-rígidas com placa de extremidade estendida submetidas a momento fletor e esforço normal. In *CILAMCE XXVI - The Iberian Latin American Congress on Computational Methods in Engineering*, volume 1, pages 1–13, Guarapari - Espírito Santo - Brasil, 2005.

[5] L. S. da Silva, L. R. O. de Lima, P. C. G. da S. Vellasco, and S. A. L. de Andrade. Behaviour oj flush endplate beam-to-column joints under bending and axial force. *International Journal of Steel and Composite Structures*, 4(2):77–94, 2004.

[6] L. Simões da Silva and A. G. Coelho. A analytical evaluation of the response of steel joints under bending and axial force. *Computers & Structures*, 79:873–881, 2000.

[7] L. R. O. de Lima, L. S. da Silva, P. C. G. da S Vellasco, and S. A. L. de Andrade. Experimental evaluation of extended endplate beam-to-column joints subjected to bending and axial force. *Engineering Structures*, 46(7):1–15, 2004.

[8] J. P. Jaspart. Recent advances in the field of steel joints column bases and further configurations for beam-to-column joints and beam splices. *Chercheur qualifié du F.N.R.S.*, page 353, 1997.

[9] J.P. Jaspart, M. Braham, and F. Cerfontaine. Strength of joints subjected to combined action of bending moment and axial force. In *Conference Eurosteel '99*, CVUT Praha - Czech Republic, May 26-29 1999.

[10] F. Laurent. Influence de l'effort normal sur lê calcul des assemblages semi-rigides. *Universite Blaise Pascal*, 1994. 114 f. CUST – Mémoire presente en vue de l'obtention du diplome d'ingénieur.

[11] Eurocode 3 prEN 1993-1.8. Design of steel structures – part 1.8: Design of joints ("final draft") - cen,. European Committee for Standardisation, Brussels, 2003.

[12] F. Wald and M. Švarc. Experiments with end plate joints subject to moment and normal force. CTU Reports 2-3, Contributions to Experimental Investigation of Engineering Materials and Structures, Prague, 2001.